

Chiral-loop-current and geometry-driven anisotropic nonreciprocal transport in kagome superconductor CsV_3Sb_5

Yuda Zhang(张钰达), Xiangqi Liu(刘祥麒), Hanlin Lu(卢瀚林), Chang Jiang(蒋昶), Xiangyu Cao(曹翔宇), Qiang Ma(马强), Yanfeng Guo(郭艳峰), Faxian Xiu(修发贤)

Citation: Chin. Phys. B. 35, 097303 (2026). DOI: 10.1088/1674-1056/ae71b1 |
CSTR: 32038.14.CPB.ae71b1
http://cpb.iphy.ac.cn; http://iopscience.iop.org/cpb

What follows is a list of articles you may be interested in

Emergent ferroelectricity in the two-dimensional Janus MoSSe monolayer driven by nondegenerate phonon instability

Zhi-Long Cao(曹智龙), Chen Cao(曹琛), Jia-Jun Xu(徐佳俊), Jia-Xu Yan(闫家旭), Lei Liu(刘雷), De-Zhen Shen(申德振)

Chin. Phys. B. 34, 117305 (2025). DOI: 10.1088/1674-1056/ae0d57 | CSTR: 32038.14.CPB.ae0d57

Current density in anomalous Hall effect regime under weak scattering

Ning Dai(戴凝), Bin Zhou(周斌)

Chin. Phys. B. 34, 077301 (2025). DOI: 10.1088/1674-1056/adcd42 | CSTR: 32038.14.CPB.adcd42

Scanning tunneling microscopy study on symmetry breaking of charge density wave in FeGe

Jiakang Zhang(张嘉康), Ziyuan Chen(陈子元), Xueliang Wu(吴学良), Mingzhe Li(李明哲), Yuanji Li(李元骥), Ruotong Yin(尹若彤), Jiashuo Gong(巩佳硕), Shiyuan Wang(王适源), Aifeng Wang(王爱峰), Dong-Lai Feng(封东来), Ya-Jun Yan(闫亚军)

Chin. Phys. B. 34, 047303 (2025). DOI: 10.1088/1674-1056/adb389 | CSTR: 32038.14.CPB.adb389

Correlated physics, charge and magnetic orders in moiré kagomé systems

Zhaochen Liu(刘兆晨), Jing Wang(王靖)

Chin. Phys. B. 34, 027304 (2025). DOI: 10.1088/1674-1056/ad9ffa | CSTR: 32038.14.CPB.ad9ffa

Chiral phonons of honeycomb-type bilayer Wigner crystals

Dingrui Yang(杨丁睿), Lingyi Li(李令仪), Na Zhang(张娜), Hongyi Yu(俞弘毅)

Chin. Phys. B. 34, 017301 (2025). DOI: 10.1088/1674-1056/ad8eca | CSTR: 32038.14.CPB.ad8eca

---

RAPID COMMUNICATION

Chiral-loop-current and geometry-driven anisotropic nonreciprocal transport in kagome superconductor CsV_3Sb_5

Yuda Zhang(张钰达)[1,2,†], Xiangqi Liu(刘祥麒)[3,†], Hanlin Lu(卢瀚林)[1,2,†], Chang Jiang(蒋昶)[1,2], Xiangyu Cao(曹翔宇)[1,2], Qiang Ma(马强)[1,2], Yanfeng Guo(郭艳峰)[3,4,‡], and Faxian Xiu(修发贤)[1,2,5,6,§]

[1] *State Key Laboratory of Surface Physics and Department of Physics, Fudan University, Shanghai* 200433, *China*
[2] *Shanghai Research Center for Quantum Sciences, Shanghai* 201315, *China*
[3] *State Key Laboratory of Quantum Functional Materials, School of Physical Science and Technology, ShanghaiTech University, Shanghai* 201210, *China*
[4] *ShanghaiTech Laboratory for Topological Physics, ShanghaiTech University, Shanghai* 201210, *China*
[5] *Institute for Nanoelectronic Devices and Quantum Computing, Fudan University, Shanghai* 200433, *China*
[6] *Zhangjiang Fudan International Innovation Center, Fudan University, Shanghai* 201210, *China*

(Received 16 April 2026; revised manuscript received 20 May 2026; accepted manuscript online 22 May 2026)

Nonreciprocal transport phenomena serve as direct probes of symmetry breaking in quantum materials. The layered kagome metal CsV_3Sb_5 undergoes a charge-density-wave (CDW) transition, below which a chiral-loop-current order emerges, breaking time-reversal and inversion symmetries. Here, we report the observation of pronounced nonreciprocal charge transport in exfoliated thin flakes of CsV_3Sb_5, and systematically examine its anisotropy to map the symmetry-breaking pattern. We develop a phenomenological model that captures the role of chiral loop currents and current inhomogeneity in generating the nonreciprocal response. The nonreciprocal signal is strongly suppressed in Ta-doped CsV_3Sb_5, where the CDW phase is absent, confirming its intimate connection to the chiral ordered state. Our results reveal the symmetry breaking in the kagome superconductor CsV_3Sb_5 via nonreciprocal transport and highlight the profound connection between chirality and nonreciprocal transport.

Keywords: nonreciprocal transport, kagome superconductor, symmetry breaking

PACS: 73.50.–h, 72.20.Ht, 72.10.Di

DOI: 10.1088/1674-1056/ae71b1 **CSTR:** 32038.14.CPB.ae71b1

1. Introduction

The kagome superconductor CsV_3Sb_5 family exhibits numerous extraordinary quantum phenomena, making it a prominent platform for strongly correlated physics. The geometrically frustrated kagome vanadium lattice contributes to the anomalous Hall effect.[1–3] The strongly correlated behavior leads to superconductivity,[4–6] with evidence of time-reversal symmetry breaking.[7–9] Furthermore, scanning tunneling microscopy (STM) reveals that below the charge-density-wave (CDW) transition temperature, an intrinsic chirality develops associated with a $3q$ CDW phase,[10–13] which has also been confirmed by x-ray scattering experiments.[14] Other studies have also shown a similar flux phase around this temperature range.[15–17] From a theoretical perspective, chirality originates from the charge loop current that breaks time-reversal symmetry and can be tuned by an external magnetic field perpendicular to the kagome plane. Meanwhile, the CDW is found to arise from a $2c$ stacking order of the adjacent kagome layers, leading to the breaking of the six-fold rotational symmetry.[18] Some researchers also claim the existence of an electronic nematic phase, which can also break the six-fold rotational symmetry.[16,19,20] Although the underlying mechanism still needs further study, various experiments, including superconducting property anisotropy, resistance anisotropy, and in-plane magnetoresistance anisotropy,[21–23] have confirmed the rotational symmetry breaking inside this system.

The symmetry breaking below the CDW transition temperature makes the CsV_3Sb_5 family a promising platform for nonreciprocal transport. The nonreciprocal transport of KV_3Sb_5 under out-of-plane current and a nearly in-plane field has been reported.[24] Recently, nonreciprocal transport with in-plane current and out-of-plane magnetic field has also been detected in CsV_3Sb_5,[25] in which they attribute the nonreciprocal resistance to a mixed influence of the chiral loop current and a geometric factor, the nonuniform current distribution. Although the nonreciprocal transport has already been studied in this system, the symmetry analysis of the nonreciprocal transport and the direct connection between the nonreciprocal transport and the chiral loop current phase are still lacking.

[†]These authors contributed equally to this work.
[‡]Corresponding author. E-mail: guoyf@shanghaitech.edu.cn
[§]Corresponding author. E-mail: Faxian@fudan.edu.cn

© 2026 Chinese Physical Society and IOP Publishing Ltd. All rights, including for text and data mining, AI training, and similar technologies, are reserved.

Chemical substitution provides an effective means to tune these intertwined electronic orders. Atomic replacement of vanadium significantly influences the stability of the CDW and superconducting phases. Ta doping suppresses the CDW order while enhancing superconductivity, whereas Mo doping weakens superconductivity and increases the CDW transition temperature.[26–29] Such tunability has enabled systematic investigations of the microscopic mechanisms underlying the CDW and the associated chiral loop current phase.

In this work, we fabricated CsV_3Sb_5 thin flakes into a circular disk geometry, which is particularly advantageous for the symmetry analysis. The circular disk shape induces a geometric current imbalance, which, together with the chiral loop current, contributes to the nonreciprocal transport. In this device, we observe a second-harmonic resistance exhibiting a cubic relationship with the magnetic field. We provide a phenomenological model to understand the origin of the nonreciprocal resistance. When rotating the direction of the applied current and measuring electrodes, we found a significant twofold symmetry in the second harmonic resistance of CsV_3Sb_5, which shows similar anisotropy with the superconducting transition onset temperature and the first harmonic resistance in the normal state in this sample. Furthermore, we demonstrate that the cubic nonreciprocal response disappears in Ta-doped CsV_3Sb_5, in which the CDW phase is suppressed, confirming the crucial role of the CDW-induced chiral loop current.

2. Methods

2.1. Crystal growth and characterization

Single crystals of CsV_3Sb_5 and $CsV_{2.8}Ta_{0.2}Sb_5$ were synthesized via a self-flux method. High-purity starting materials of Cs liquid (99.98%), V powder (99.9%), Ta powder (99.99%), and Sb granules (99.999%) were combined in a 1:1:4 molar ratio, sealed in an alumina crucible within a tantalum tube under vacuum. The assembly was heated in a furnace up to 900 °C within 10 hours, kept at that temperature for 20 hours, and then slowly cooled down to 450 °C at a rate of 1.5 °C/h. Residual flux was removed through selective etching of Cs–Sb phases using ultrapure water. Crystal composition was verified by energy-dispersive x-ray spectroscopy (EDX) using a Phenom Pro SEM. The characterization of the grown crystals can be seen in supporting note 1.

2.2. Nonreciprocal transport measurement

CsV_3Sb_5 nanoflakes were exfoliated onto Si/SiO_2 substrates. A standard electron-beam lithography process was used to fabricate circular disk-shaped devices. The devices were measured using the Quantum Design Dynacool system, with a temperature range of 1.8–400 K and a maximum magnetic field of 9 T. The a.c. measurement was carried out with a Keithley 6221 as the current source and a Stanford Research Systems SR860 for the first harmonic voltage V^{ω} and second harmonic voltage $V^{2\omega}$ measurement. The d.c. measurement was carried out with an Agilent AG2902A as the current source and a Keithley 2182 nanovoltmeter for voltage measurement.

3. Results and discussion

CsV_3Sb_5 thin films were mechanically exfoliated onto SiO_2/Si substrates, and the circular-disk-shaped electrodes were fabricated using standard electron-beam lithography. The crystal structure is shown in Fig. 1(a), and the vanadium kagome plane lies in the substrate plane. Figure 1(b) shows a sketch of the measurement geometry. The current is applied between two opposite electrodes, and the first harmonic and second harmonic resistances were measured at the right and left sides of the current direction. Figure 1(c) shows the second harmonic resistance as a function of the magnetic field at 5 K after antisymmetrization to exclude the magnetic field symmetric thermoelectric contribution. For magneto-chiral anisotropy systems, the second harmonic resistance follows

$$R^{2\omega} = \gamma RIB.$$

Here, R stands for the normal resistance, I is the applied current, B is the external magnetic field, and γ stands for the coefficient of magneto-chiral anisotropy. According to this equation, the second harmonic resistance normally exhibits a linear relationship with the magnetic field, which is the situation for most systems with nonreciprocal transport. In CsV_3Sb_5, however, the second-harmonic resistance exhibits a cubic dependence on magnetic field with opposite signs on the left and right sides of the device. Second harmonic signals from other extrinsic effects have been ruled out to make our results more convincing (see supporting note 2). The second harmonic transport in CsV_3Sb_5 is significantly different from normal symmetry-breaking systems and imitates the behavior of nonreciprocal transport in systems with chiral edge states.[30–32]

To gain a better understanding of this behavior, we provide a theoretical model that derives the nonreciprocal transport in the CsV_3Sb_5 circular disk phenomenologically. The coupling between the flowing carriers and the localized chiral loop current can be interpreted as

$$\omega(r) \propto \boldsymbol{J} \cdot \boldsymbol{I}_{\mathrm{lc}}.$$

Here, $\boldsymbol{J}$ stands for the applied current, which represents the flowing carriers, and $\boldsymbol{I}_{\mathrm{lc}}$ indicates the chiral loop current which flows locally in the kagome plane. When the applied current is parallel to the chiral loop current, the coupling is stronger and scattering is less likely to happen; when the applied current is

antiparallel to the chiral loop current, the scattering process is reversed. The loop current term can be rewritten as

$$\boldsymbol{I}_{\rm lc} = \nabla \times \boldsymbol{A}_{\rm lc}.$$

Here, $\boldsymbol{A}_{\rm lc}$ is the vector potential for the chiral loop current, which has a connection to the orbital magnetism $\boldsymbol{m}_{\rm orb}$. Then, $\boldsymbol{\omega}(r)$ can be written as

$$\boldsymbol{\omega}(r) \propto \nabla \cdot (\boldsymbol{A}_{\rm lc} \times \boldsymbol{J}) + \boldsymbol{A}_{\rm lc} \cdot (\nabla \times \boldsymbol{J}).$$

When integrating throughout the entire measuring area, we can obtain

$$\begin{aligned} W &= \int_V \boldsymbol{\omega}(r)\mathrm{d}V \propto \int_V (\nabla \cdot (\boldsymbol{A}_{\rm lc} \times \boldsymbol{J}) + \boldsymbol{A}_{\rm lc} \cdot (\nabla \times \boldsymbol{J}))\,\mathrm{d}V \\ &= \oint (\boldsymbol{A}_{\rm lc} \times \boldsymbol{J})\,\mathrm{d}S + \int \boldsymbol{A}_{\rm lc} \cdot (\nabla \times \boldsymbol{J})\,\mathrm{d}V. \end{aligned}$$

The W can be regarded as an effective phenomenological quantity for the asymmetric scattering process, which tracks the magnitude of the nonreciprocal transport. The current distribution is spatially nonuniform and therefore the term $\nabla \times \boldsymbol{J}$ is not strictly zero in the sample, especially around the edge and contact area. However, the current curl should be negligible around the measuring channel. And the integration would counteract the opposite current curl around the source and drain. Thus, the second term should only be a secondary correction, and the first term dominates. So, from this point of view, the divergence of the vector product between the vector potential for the chiral loop current and the applied current contributes to the nonreciprocal transport in this system. From this model, we understand that chiral nonreciprocal transport in the CsV_3Sb_5 system originates from the chiral loop current, together with a nonuniform current distribution. The evolution of the chiral loop current phase under external magnetic fields induces a nonlinear relationship between the nonreciprocal resistance and the magnetic field. The nonuniformity of the applied current along the right and left sides results in opposite signs in the nonreciprocal resistance on two sides, which imitates the scattering process in systems with a chiral edge state. Figure 1(d) provides a sketch of the nonreciprocal transport process on the left side with a negative magnetic field. The disk-shaped device induces current nonuniformity in the sample, higher current density in the middle (blue arrow) and lower density around the edge (light blue arrow). Under positive current, the scattering in the middle is strong, while the scattering is weaker around the edge, behaving as a high resistance state. When the current direction is reversed, the scattering is weakened in the middle and promoted around the edge, resulting in a low resistance state. Under this situation, we should get a positive nonreciprocal resistance on the left side, which is exactly what we derived from transport measurement. The nonreciprocal transport at the right side or under a positive magnetic field is just the opposite of this. From this view, we can understand the field-antisymmetric nonreciprocal resistance in the CsV_3Sb_5 circular disk sample.

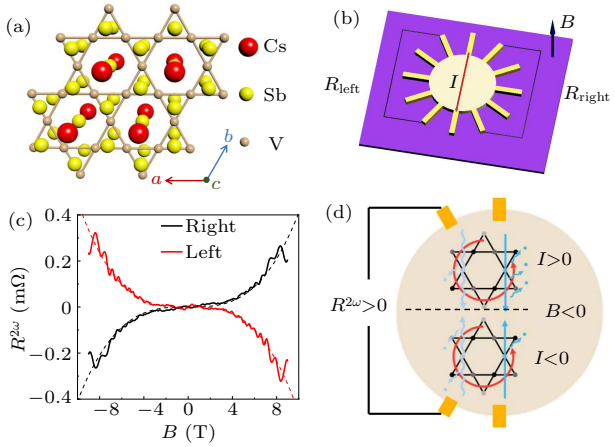


Fig. 1. Nonuniform current distribution and chiral loop phase-mediated nonreciprocal resistance in the kagome superconductor CsV_3Sb_5. (a) Crystal structure of the kagome superconductor CsV_3Sb_5. The brown V–V bonds form the kagome plane of the CsV_3Sb_5. The crystal axis is marked in red (a axis), blue (b axis), and green (c axis). (b) A sketch diagram of the measurement geometry. The electrodes, fabricated into a round shape, form the circular-disk-shaped device. The current was applied between two opposite electrodes, and the longitudinal resistance was measured along the right and left sides of the current. The magnetic field was applied perpendicularly to the sample plane. (c) Antisymmetrized second-harmonic resistance of the CsV_3Sb_5 circular disk device at 5 K, shown for the right (black) and left (red) sides. The nonreciprocal resistance exhibits opposite signs and a cubic magnetic-field dependence, as indicated by the dotted fitting curves. (d) A cartoon to explain the origin of the nonreciprocal resistance in the CsV_3Sb_5 circular disk under a negative magnetic field. The current flows along the two electrodes in opposite directions. The disk-shaped device induces current nonuniformity, marked by the depth of the color (blue and light blue). The different scattering processes for positive and negative current directions induce a positive second harmonic signal at the left side, which is consistent with our experimental results.

After deriving the nonreciprocal resistance in CsV_3Sb_5, we measured the evolution of the nonreciprocal resistance under different current directions. Figure 2(a) shows the measurement geometry of the angular-dependent measurement. We set 0° in our measurement at the electrode perpendicular to one axis of the thin flake, as distinguished under an optical microscope. The nonreciprocal resistance at different current directions under multiple magnetic fields is shown in Fig. 2(b). A clear two-fold symmetry in nonreciprocal resistance can be seen, and the anisotropy is preserved under a 3 T magnetic field. Figure 2(c) illustrates the symmetry of several parameters derived from transport measurements, including nonreciprocal resistance at 5 K, 9 T, normal-state first harmonic resistance at 5 K, 0 T, and the superconducting transition onset temperature. All these parameters exhibit a two-fold symmetry. The peaks of the nonreciprocal resistance and superconducting transition temperature, the dips of the normal state resistance, aligned in a similar direction around 30°. This anisotropy agrees well with the theory of 2c stacking of the 3q CDW phase and the electronic nematicity.[18,19] Due to the establishment of the CDW phase and possible electronic nematicity, the six-fold rotational symmetry is broken, and a

two-fold symmetry is oriented along one of the crystal axes (*a* or *b* axis in Fig. 1(a)), which deviates by 30° from our angle definition. A similar CsV_3Sb_5 circular disk sample shown in the supplementary material exhibits a similar anisotropy (supporting note 3). The peak of the nonreciprocal resistance occurs at 0°, which is consistent with the fact that the 0° electrode is defined as the electrode parallel to the crystal axes. These samples confirm that the anisotropy originates from intrinsic symmetry breaking associated with the CDW phase rather than arbitrary electrode misalignment.

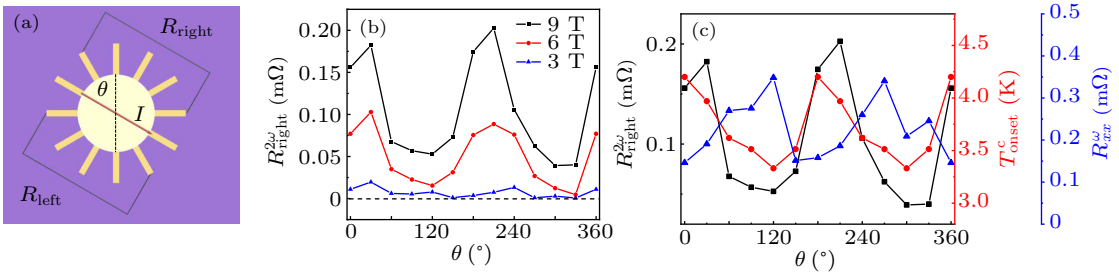


Fig. 2. Two-fold symmetric nonreciprocal resistance in the CsV_3Sb_5 circular disk. (a) A schematic diagram of the measuring geometry. The zero-degree current direction is defined perpendicular to one crystallographic axis identified under an optical microscope. (b) The current-direction-dependent nonreciprocal resistance in CsV_3Sb_5 circular disk. A pronounced two-fold symmetry is observed and remains robust up to 3 T. The maximum nonreciprocal resistance occurs around 30° and 210°, corresponding to one of the crystal axes (*a* axis or *b* axis). (c) Angular dependence of the second-harmonic resistance (black), first-harmonic resistance (blue), and superconducting onset temperature (red). All three quantities exhibit consistent two-fold symmetry. The peak value of the nonreciprocal resistance and superconducting onset temperature, the minimum value of the first harmonic resistance, align around 30°, indicating the intrinsic origin of the anisotropy.

Next, we measured the nonreciprocal resistance of the CsV_3Sb_5 circular disk under various current amplitudes. Figure 3(a) displays the first harmonic voltage of the right and left sides of the sample at 5 K and no external field. The linear dependence of the first-harmonic voltage versus the current amplitude indicates a negligible change in the transport properties in the device under various current amplitudes and confirms the minor contribution from current heating and other side effects in this sample. The slight deviation of the first harmonic voltage on the right and left sides mainly originates from the inevitable misalignment of the electrode during the nanofabrication process. Figure 3(b) shows the second harmonic voltage of the right and left sides of the sample at 5 K, 9 T, when the current is applied along 0°. The second harmonic voltage scales quadratically with the current amplitude, revealing the intrinsic nonlinear origin of the second harmonic signal. The nonreciprocal voltage also shows opposite signs on the right and left sides of the current. Furthermore, the second harmonic voltage at different current directions is shown in Fig. 3(c). The nonreciprocal voltages under different current directions all exhibit the quadratic scaling with the current amplitude, which further verifies our result on the anisotropy of nonreciprocal transport.

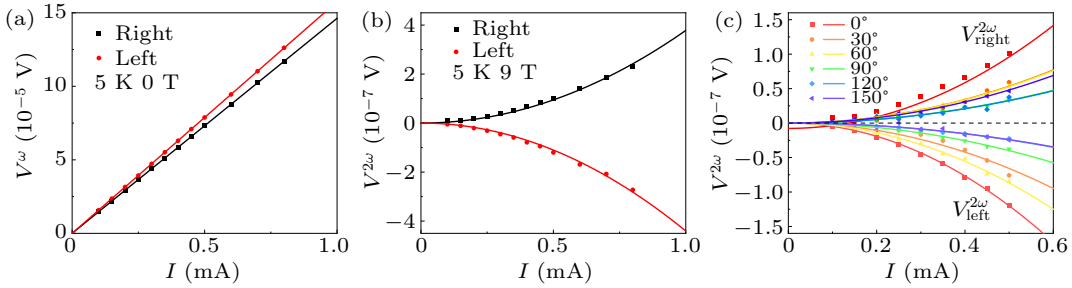


Fig. 3. Current-dependent nonreciprocal transport in the CsV_3Sb_5 circular disk. (a) First-harmonic voltage measured on the right (black) and left (red) sides as a function of current amplitude at 5 K and 0 T. The linear dependence indicates a negligible change in the transport properties under different current amplitudes. (b) Second harmonic voltage as a function of the current amplitude at 5 K, 9 T. The quadratic dependence confirms the intrinsic nonlinear origin of the nonreciprocal signal. The sign of the nonreciprocal voltage is different on the right side and left side. The data in (a) and (b) were measured at 0°. (c) Second-harmonic voltage versus current amplitude for different current directions. All curves display quadratic scaling and opposite polarities on the two sides, further demonstrating the reliability of the anisotropic nonreciprocal transport.

Considering the origin of the nonreciprocal resistance in CsV_3Sb_5, the non-uniform current distribution and chiral loop phase are both crucial for the detection of the nonreciprocal resistance. Thus, the absence of either feature should make the B^3-related nonreciprocal resistance vanish. To verify the CDW origin of the cubic nonreciprocal response, we compare the nonreciprocal resistance in the CsV_3Sb_5 sample and a Ta-doped $CsV_{2.8}Ta_{0.2}Sb_5$ circular disk device. The Ta-doping restrains the CDW phase in CsV_3Sb_5,[29] and the corresponding chiral loop phase should also be suppressed. Figures 4(a) and 4(c) illustrate the temperature-dependent resistance and the differential resistance with respect to the temperature (dR/dT) for the CsV_3Sb_5 device measured above (Fig. 4(a)) and a $CsV_{2.8}Ta_{0.2}Sb_5$ (Fig. 4(c)) circular disk de-

vice. The R–T curve in the CsV_3Sb_5 sample shows a kink, and the dR/dT rises sharply at around 82 K, indicating the CDW transition. For the $CsV_{2.8}Ta_{0.2}Sb_5$ sample, however, no obvious CDW transition can be seen in the entire temperature range, suggesting the complete suppression of a long-range CDW phase. Figures 4(b) and 4(d) show the nonreciprocal coefficient as a function of the magnetic field at 5 K for two samples. The nonreciprocal coefficient γ for the CsV_3Sb_5 circular disk displays a quadratic relation with the magnetic field, consistent with the B^3-related nonreciprocal resistance. And opposite signs can be seen along the right and left sides of the current. However, for the $CsV_{2.8}Ta_{0.2}Sb_5$ circular disk, the nonreciprocal coefficient is significantly different from that of CsV_3Sb_5. The nonreciprocal coefficient shows no evolution under magnetic fields. The B-linear nonreciprocal resistance in an inversion-symmetry-preserved system is most likely a thermoelectric contribution. The joule heating from the source and drain electrodes results in a high temperature spot on the edge and a low temperature spot in the middle of the sample, thus inducing a Nernst-like field-antisymmetric nonreciprocal signal in the longitudinal direction.[33] With these results, we confirm that the B^3-related nonreciprocal resistance in the CsV_3Sb_5 circular disk is closely related to the CDW and chiral loop phase. When the CDW was suppressed, the B^3-related nonreciprocal resistance also vanished.

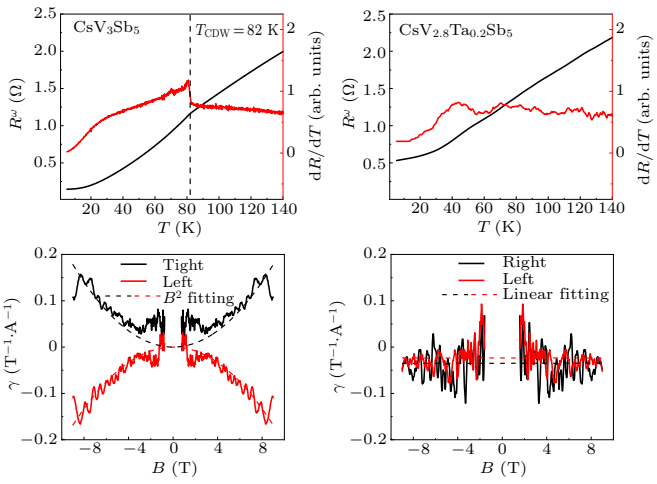


Fig. 4. CDW transition-dependent nonreciprocal transport in the CsV_3Sb_5 series. (a) Temperature-dependent resistance and the corresponding differential resistance with respect to the temperature (dR/dT) of the undoped CsV_3Sb_5 sample measured above. The kink in the R–T curve and a sharp peak in the dR/dT indicate the CDW transition in CsV_3Sb_5 at 82 K. (b) Magnetic field dependence of the nonreciprocal coefficient γ for CsV_3Sb_5. A quadric field-dependence with opposite signs on the left and right sides can be seen. (c) Temperature-dependent resistance and the corresponding differential resistance with respect to the temperature of the Ta-doped $CsV_{2.8}Ta_{0.2}Sb_5$ circular disk sample. No CDW transition is seen in either the R–T curve or the dR/dT curve, suggesting the suppression of the CDW phase under Ta-doping. (d) Magnetic-field dependence of the nonreciprocal coefficient γ for $CsV_{2.8}Ta_{0.2}Sb_5$. No obvious evolution of the nonreciprocal coefficient under the magnetic field is present, distinct from the behavior of the undoped CsV_3Sb_5 sample.

4. Conclusion

In conclusion, we fabricated the kagome superconductor CsV_3Sb_5 circular disk device and found a B^3-scaled nonreciprocal resistance. We developed a theoretical model to understand the contributions of nonuniform current distribution and the chiral loop phase to the B^3-scaled nonreciprocal resistance. Due to the symmetry-breaking induced by the development of the CDW phase and chiral loop current, the nonreciprocal resistance shows a two-fold symmetry consistent with the crystal axes of the CsV_3Sb_5. Furthermore, for Ta-doped CsV_3Sb_5, the suppression of the CDW phase leads to the vanishing of the B^3-dependent nonreciprocal resistance. With these results, we highlight the importance of the chiral loop phase to the nonreciprocal transport in the CsV_3Sb_5 system.

Acknowledgements

F. X. was supported by the National Natural Science Foundation of China (Grant No. 52225207), the Shanghai Pilot Program for Basic Research-Fudan University 21TQ1400100 (Grant No. 21TQ006), and the Shanghai Municipal Science and Technology Major Project (Grant No. 2019SHZDZX01). Part of the sample fabrication was performed at Fudan Nano-fabrication Laboratory.

References

[1] Yang S Y, Wang Y, Ortiz B R, Liu D, Gayles J, Derunova E, Gonzalez-Hernandez R, Šmejkal L, Chen Y, Parkin S S P, Wilson S D, Toberer E S, McQueen T and Ali M N 2020 *Sci. Adv.* **6** eabb6003

[2] Yu F H, Wu T, Wang Z Y, Lei B, Zhuo W Z, Ying J J and Chen X H 2021 *Phys. Rev. B* **104** L041103

[3] Wang L, Zhang W, Wang Z, Poon T F, Wang W, Tsang C W, Xie J, Zhou X, Zhao Y, Wang S, Lai K T and Goh S K 2023 *J. Phys. Mater.* **6** 02LT01

[4] Ortiz B R, Gomes L C, Morey J R, Winiarski M, Bordelon M, Mangum J S, Oswald I W H, Rodriguez-Rivera J A, Neilson J R, Wilson S D, Ertekin E, McQueen T M and Toberer E S 2019 *Phys. Rev. Mater.* **3** 094407

[5] Ortiz B R, Teicher S M L, Hu Y, Zuo J L, Sarte P M, Schueller E C, Abeykoon A M M, Krogstad M J, Rosenkranz S, Osborn R, Seshadri R, Balents L, He J and Wilson S D 2020 *Phys. Rev. Lett.* **125** 247002

[6] Du F, Luo S, Ortiz B R, Chen Y, Duan W, Zhang D, Lu X, Wilson S D, Song Y and Yuan H 2021 *Phys. Rev. B* **103** L220504

[7] Le T, Pan Z, Xu Z, Liu J, Wang J, Lou Z, Yang X, Wang Z, Yao Y, Wu C and Lin X 2024 *Nature* **630** 64

[8] Wang S, Feng X, Fang J Z, Peng J P, Sun Z T, Yang J J, Liu J, Zhao J J, Wang J K, Liu X J, Wu Z N, Sun S, Kang N, Wu X S, Zhang Z, Fu X, Law K T, Lin B C and Yu D 2026 *Nat. Commun.* **17** 1310

[9] Le T, Xu Z, Liu J, Zhan R, Wang Z and Lin X 2025 *Phys. Rev. Lett.* **135** 096002

[10] Jiang Y X, Yin J X, Denner M M, Shumiya N, Ortiz B R, Xu G, Guguchia Z, He J, Hossain M S, Liu X, Ruff J, Kautzsch L, Zhang S S, Chang G, Belopolski I, Zhang Q, Cochran T A, Multer D, Litskevich M, Cheng Z J, Yang X P, Wang Z, Thomale R, Neupert T, Wilson S D and Hasan M Z 2021 *Nat. Mater.* **20** 1353

[11] Shumiya N, Hossain Md S, Yin J X, Jiang Y X, Ortiz B R, Liu H, Shi Y, Yin Q, Lei H, Zhang S S, Chang G, Zhang Q, Cochran T A, Multer D, Litskevich M, Cheng Z J, Yang X P, Guguchia Z, Wilson S D and Hasan M Z 2021 *Phys. Rev. B* **104** 035131

[12] Wang Z, Jiang Y X, Yin J X, Li Y, Wang G Y, Huang H L, Shao S, Liu J, Zhu P, Shumiya N, Hossain M S, Liu H, Shi Y, Duan J, Li X, Chang G, Dai P, Ye Z, Xu G, Wang Y, Zheng H, Jia J, Hasan M Z and Yao Y 2021 *Phys. Rev. B* **104** 075148

[13] Feng X, Jiang K, Wang Z and Hu J 2021 *Sci. Bull.* **66** 1384

[14] Elmers H J, Tkach O, Lytvynenko Y, Yogi P, *et al*. 2025 *Phys. Rev. Lett.* **134** 096401

[15] Mielke C, Das D, Yin J X, Liu H, Gupta R, Jiang Y X, Medarde M, Wu X, Lei H C, Chang J, Dai P, Si Q, Miao H, Thomale R, Neupert T, Shi Y, Khasanov R, Hasan M Z, Luetkens H and Guguchia Z 2022 *Nature* **602** 245

[16] Asaba T, Onishi A, Kageyama Y, Kiyosue T, Ohtsuka K, Suetsugu S, Kohsaka Y, Gaggl T, Kasahara Y, Murayama H, Hashimoto K, Tazai R, Kontani H, Ortiz B R, Wilson S D, Li Q, Wen H H, Shibauchi T and Matsuda Y 2024 *Nat. Phys.* **20** 40

[17] Gui H, Yang L, Wang X, Chen D, Shi Z, Zhang J, Wei J, Zhou K, Schnelle W, Zhang Y, Liu Y, Bangura A F, Wang Z, Felser C, Yuan H and Jiao L 2025 *Nat. Commun.* **16** 4275

[18] Jin F, Ren W, Tan M, Xie M, Lu B, Zhang Z, Ji J and Zhang Q 2024 *Phys. Rev. Lett.* **132** 066501

[19] Nie L, Sun K, Ma W, Song D, Zheng L, Liang Z, Wu P, Yu F, Li J, Shan M, and others 2022 *Nature* **604** 59

[20] Li H, Cheng S, Ortiz B R, Tan H, Werhahn D, Zeng K, Johrendt D, Yan B, Wang Z, Wilson S D and Zeljkovic 2023 *Nat. Phys.* **19** 1591

[21] Ni S, Ma S, Zhang Y, Yuan J, Yang H, Lu Z, Wang N, Sun J, Zhao Z, Li D, Liu S, Zhang H, Chen H, Jin K, Cheng J, Yu L, Zhou F, Dong X, Hu J, Gao H J and Zhao Z 2021 *Chin. Phys. Lett.* **38** 057403

[22] Lou H X, Ye X G, Liao X, Zhao T Y, Wang A Q, Yu D P and Liao Z M 2024 *Appl. Phys. Lett.* **125** 132601

[23] Xiang Y, Li Q, Li Y, Xie W, Yang H, Wang Z, Yao Y and Wen H H 2021 *Nat. Commun.* **12** 6727

[24] Guo C, Putzke C, Konyzheva S, Huang X, Gutierrez-Amigo M, Errea I, Chen D, Vergniory M G, Felser C, Fischer M H, Neupert T and Moll P J W 2022 *Nature* **611** 461

[25] Xu L, Xie Z, Wang J, Yin Q, Lei H and Zhang J 2025 *Nano Lett.* **25** 14222

[26] Liu M, Han T, Hu X, Tu Y, Zhang Z, Long M, Hou X, Mu Q and Shan L 2022 *Phys. Rev. B* **106** L140501

[27] Zhu K J, Nie L P, Lei B, Wang M J, Sun K L, Deng Y Z, Tian M L, Wu T and Chen X H 2024 *Phys. Rev. Res.* **6** 023295

[28] Song J, Han T, Zhou Z, Mu Q, Hou X, Zhang Z, Tu Y and Shan L 2024 *Phys. Rev. B* **110** 054518

[29] Liu J, Li Q, Li Y, Fan X, Li J, Zhu P, Deng H, Yin J X, Yang H, Li J, Wen H-H and Wang Z 2024 *Sci. Rep.* **14** 9580

[30] Zhang Z, Wang N, Cao N, Wang A, Zhou X, Watanabe K, Taniguchi T, Yan B and Gao W 2022 *Nat. Commun.* **13** 6191

[31] Yasuda K, Morimoto T, Yoshimi R, Mogi M, Tsukazaki A, Kawamura M, Takahashi K S, Kawasaki M, Nagaosa N and Tokura Y 2020 *Nat. Nanotechnol.* **15** 831

[32] Li C, Wang R, Zhang S, Qin Y, Ying Z, Wei B, Dai Z, Guo F, Chen W, Zhang R, Wang B, Wang X and Song F 2024 *Nat. Mater.* **23** 1208

[33] Zhang C, Yuan X, Zhang J, Leng P, Mou Y, Ni Z, Zhang H, Yu C, Yang Y and Xiu F 2021 *Phys. Rev. Appl.* **15** 034084